Advances in Computer Science and Information Technology (ACSIT)
p-ISSN: 2393-9907; e-ISSN: 2393-9915; Volume 3, Issue 2; January-March, 2016, pp. 64-71

http://www.krishisanskriti.org/Publication.html

Effect of Blue Component Stars in Parameters of *NGC 6866*

Gireesh C. Joshi

P.P.S.V.M. I. College Nanakmatta, U. S. Nagar-262311
E-mail: gchandra.2012@rediffmail.com

Abstract—*The open star clusters (OSC) are important tracers for understanding the Galactic evolution. The parametric study of these astronomical-objects is crucial task due to the appearing sequence of the members of OSC. These members are defined through the various approaches such as photometric, statistical, kinematics etc. In the present paper, we have been using the photometric colours of the identified stars for categorized them into the blue and red component groups and identification of these groups is possible through (B-V) vs V colour magnitude diagram (CMD). Furthermore, the influence/effect of these groups is also examined in the estimation of cluster parameters. The stellar enhancement of cluster NGC 6866 is found through the blue-component-stars (BCS) and the linear solution of best fitted values of King Models of the radial-density-profile (RDP) gives the core radius as 5.22+/-0.29 arcmin. The good agreement of present estimated parameters of the cluster with the literature seems to be an effective evidence to consider BCS as the true representative of the cluster. The stellar distribution of the cluster shows continuous phenomena of the mass segregation. An effect of the incompleteness of photometric data is related to the mass-function slope values, which is found to be -3.80+/-0.11 and also shows the incremental nature with the incompleteness.*

Keywords*: (Galaxy): Open star cluster; individual: NGC 6866, blue component; Most probable members.*

1. INTRODUCTION

The observational study of intermediate-age open clusters (*OCs*) plays an important role to constrain the theories of stellar and Galactic evolution (Sharma et al., 2006). Though, the cluster region is also influenced by field stars (*FS*), therefore, an identification of their probable members becomes a crucial task for the parametric analysis. The influence of FS within the cluster may be occurred due to embedded position of the cluster on the Galactic disk and known as the field contamination. Furthermore, its amount depends on the location of a particular cluster on Galactic plane (Joshi et al., 2014). The scattered stellar distribution on the *CMD* leads the photometric broadening of the stellar sequence. Such broadening pattern of the *CMD* may be producing an uncertainty of fundamental parameters (reddening, distance and age) of the cluster. An accurate measurement of these parameters will be possible after the decontamination of *FS* from the *OC* and it would be carried out through either the photometric statistical criteria (Sharma et al., 2008) or the statistical cleaning in *CMDs* (Joshi et al., 2014). Recently, Joshi et al. (2015) have been introduced the statistical cleaning procedure by the colour-magnitude distance for field star, which is depends on the dimensions of grid size of *FS*. The resultant members are used to derive the fundamental parameters and examine the dynamical behaviour.

The outlines of this paper are described as following. The quality of available photometric data of cluster has been prescribed in Section 2. The separation procedure of blue and red component stars of this cluster is described in Section 3. The *RDPs* and *SNDPs* of both type stars have been described in Section 4 and Section 5, respectively. The identification procedure of giant star sequence within cluster has been discussed in Section 6. The estimation of reddening, distance and age are described in Sections 7 and 8. The MF study and examination of nature of total-to-selective-extinction are done in Sections 9 and 10 respectively. Finally, we have been summarized our results and discussed their importance in Section 11.

2. THE PREVIOUS STUDIES AND DATA

In the literature, a total of 3 photometric catalogues of deep *CCD* observations are available of this cluster, which are constructed by Joshi et al. (2012), Janes et al. (2014) and Bostanci et al. (2015). The field of view of these observations is about 13.5×13.5 $arcmin^2$, 42.8×42.8 arcmin2 and 21.5×21.5 $arcmin^2$, respectively. All authors of these catalogue have been derived the fundamental parameters. Bostanci et al. (2015) have been shown comparison of their photometry with the Joshi et al. (2012) and Janes et al. (2014) in their manuscript at Fig. 4 and Fig. 5 respectively. It seems that their photometry is matched with Janes et al. (2014). Since, Janes et al. (2014) are reported the maximum field of view of this cluster among all UBVRI catalogues, therefore, it is used to identify the blue-component-stars (BCS) and their influence in parametric analysis of the cluster.

To see the difference of stellar magnitude of common stars between Janes et al. (2014) and Joshi et al. (2012), we are cross-matched their photometric within scatter of 1 arcsec

leads 2092 common stars between both catalogues with a slope in residual magnitudes of these catalogues (as depicted in the left panels of Fig. 1). A deep investigation of figures 4 and 5 of manuscript of Bostanci et al. (2015) has clearly shown that their photometry shows approximate zero residual with Janes et al. (2014) but not for Joshi et al. (2012). Thus, unknown technical problem is present with the work of Joshi et al. (2012). Furthermore, the stellar spread of (*B-V*) vs (*U-B*) *TCD* (Fig. 1-b) is produced by those stars which having V magnitude greater than 18 mag with a upward shift (depicted by red dots) and this shifting is increased with the reddening values.

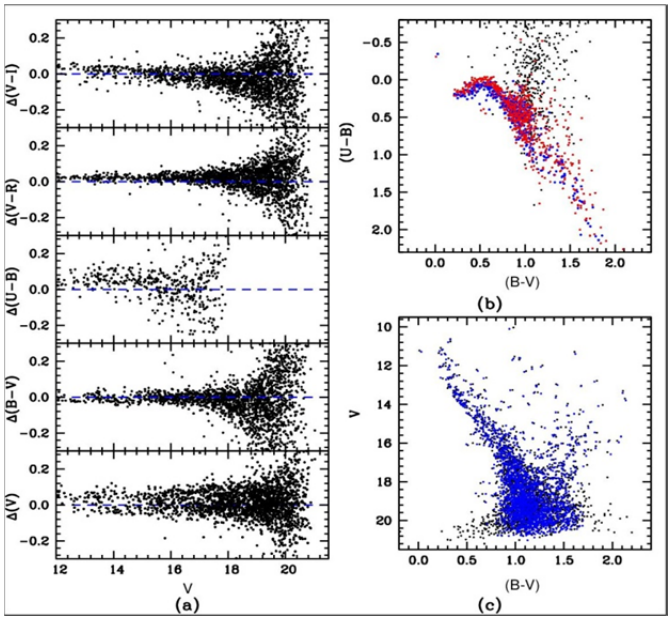

Fig. 01: ***a) Comparison of photometry catalogues between Joshi et al. (2012) and Janes et al. (2014). b) The comparison of (U-B) vs (B-V) two-colour diagrams of these catalogues. c) Here, We have also shown (B-V) vs V CMDs from both cataloges. The black and blue dots of panels (b) and (c) are represent stars from Joshi et al. (2012) and Janes et al. (2014) catalogues respectively. The red dots of panel (b) are those stars of Joshi et al. (2012) catalogue, which having V -magnitude less than 18 mag.***

The stellar distribution on the *CMD* has been depicted in the Fig. 1-c through the extracted magnitude from the both catalogue [Joshi et al. (2012) and Janes et al. (2014)] and shows similar stellar distribution except lower end of *CMD*. The reddening, *E(B-V)*, is needed to calculate the cluster distance and obtained by fitting Zero-Age-Main-Sequence [*ZAMS*, Schmidt-Kalar (1982)] in the (*U-B*) vs (*B-V*) diagram [Fig. 2]. In this figure, the black curve shows the reddened *ZAMS* which is obtained by adding a shift 0.12 mag in *E(B-V)* values of normal ZAMS. The reddened *ZAMS* is well fitted to *BCS*, whereas the red component stars (*RCS*) shows a linear trend. The linear solution of said linear pattern is computed as follows,

$$(U-B) = (1.47 \pm 0.03)(B-V) - 0.76 \pm 0.04.$$

Though, the RCS stars, having (B-V ≥1.8 mag), found to be below this linear solution and shows large slope value of (U-B)/(B-V) of RCS compare to the expected value of the clusters. The scattering of A0 type stars found to be less and stellar scattering is increasing with (B-V) except A0 type stars. The arrow indicates the normal colour excess law. Since, some RCS are also giant members of the cluster, therefore, redden ZAMS also satisfied by the pattern of RCS. Some RCS are embedded within the distribution of BCS and others RCS is below the best fitted ZAMS. The resultant reddening is found to be 0.12±0.01 mag which is slightly high from reddening (0.10 mag) estimated by Joshi et al. (2012) but close with (0.16±0.04) as derived by Janes et al. (2014) through Bayesian analysis.

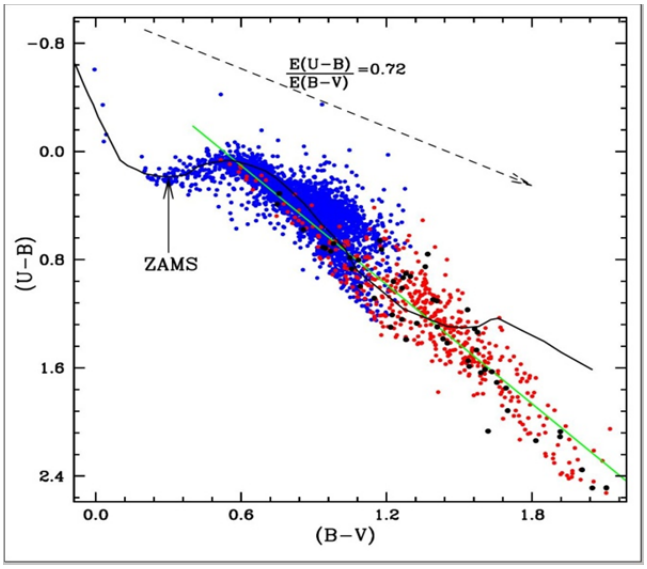

Fig. 02: ***The blue and red component stars of cluster are depicted by blue and red dots respectively. The solid black and green line represents the best fitted ZAMS on blue component stars and best linear fit in red component stars of cluster. The dashed arrow shows normal reddening law.***

3. SEPARATION PROCEDURE OF BLUE AND RED COMPONENT STARS

The stellar distribution seems to be spread out on (*B-V*) vs *V CMD* (as shown in Fig. 3 and Fig. 11). The dense stellar distribution is obtained as broad and sloppy line (left side of the above prescribed *CMD*), which may be occurred due to the probable main sequence (*MS*) of the cluster. The comparison of known literature value with the value obtained through this sequence (detailed discussion in at Section 4) provides said sequence as main-sequence (*MS*) of the cluster. Other hand, the stellar distribution of right side of *CMD (RCS)* is sparsely fulfilled. The *MS* of the cluster are separated by following linear equation of magnitude and colour,

$$V_0 = 7.66 \times (B-V)_0 + 7.32,$$

where V_o and $(B\text{-}V)_o$ are the observed magnitude and colour of stars respectively, and denoted by a black dashed arrow as

depicted in Fig. 3. The BCS and RCS are laying on the left and right sides of this arrow on the CMD plane and depicted by the blue and red dots in Fig. 3. The obtained RCS may be either super-giant members (SGM) of the cluster or field stars. The SGM are those cluster members which are evaporated from the main sequence due to the dynamical evolution. A total of 4088 and 1250 stars are found to be BCS and RCS, respectively. Since, BCS and RCS are not easily separated to each other for fainter stars more than 18.5 V-mag (Fig. 11), therefore this procedure is applicable for brighter stars from 18.5 mag in V-band. Although it seems that RCS of (V-I)/V CMD are visibly separated from the MS instead in the (B-V)/V CMD.

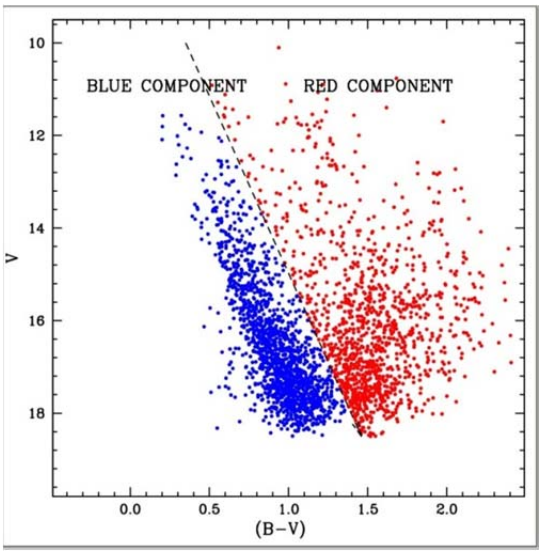

Fig. 03: The BCS and RCS have depicted by the blue and red dots. These stars are separated by the black dashed arrow.

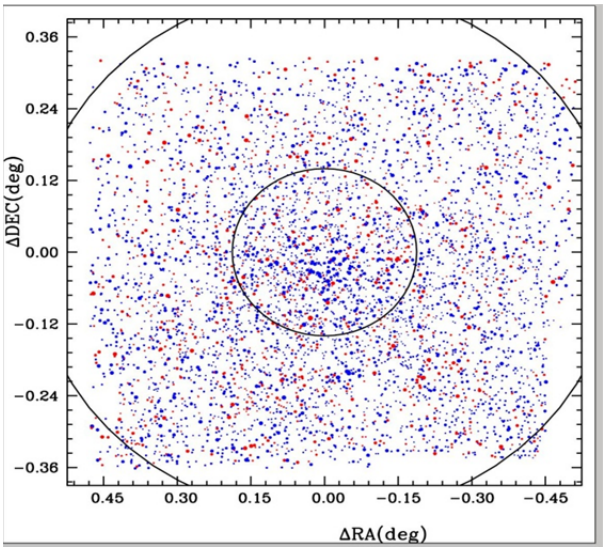

Fig. 04: The inner and outer circles represent the core radius and limiting radius of clusters. The size of the dots is proportional to their brightness. The blue and red dots are shown to be blue and red component stars respectively.

4. CLUSTER EXTENT DUE TO BLUE COMPONENT STARS

The finding chart is very effective to check out the stellar enhancement of the cluster due to either *BCS* or *RCS* as depicted in Fig. 4. In this figure, the size of dots is the function of the stellar brightness and increases towards to the brighter stars. The smallest size of dots is represented those stars which having V-magnitude to be 18.5 mag. Since, the stellar distribution of both components are seems to be present in whole observed field, therefore the radial density profile (*RDP*) of both components has been constructed to find out their role in the stellar enhancement. For this purpose, the cluster center is computed through the grid maximum count method [Joshi et al. 2015] and it comes to be 20h:03m:54.9s, +44:09:28.2, which is slightly shifted from the *SIMBAD*. For the *RDPs*, we have been computed the radial densities in the concentric rings and resultant *RDPs* are depicted in Fig. 5. These *RDPs* indicate that the stellar enhancement of the cluster occurs due to the *BCS*.

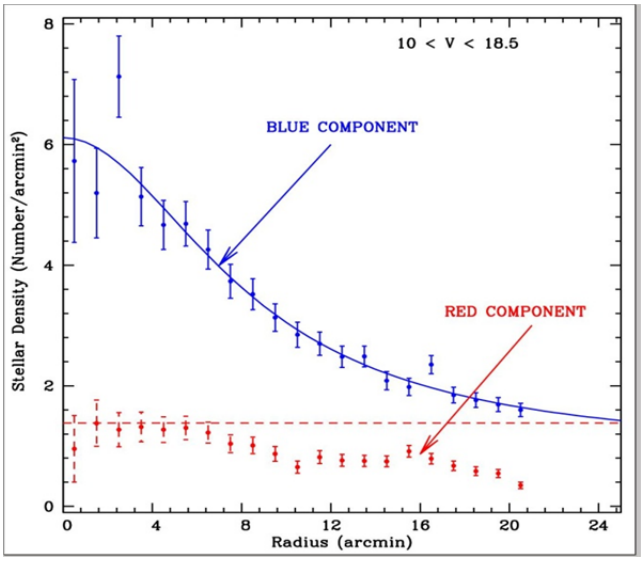

Fig. 05: The densities of BCS and RCS have been shown by blue and red dots respectively.

The following King empirical formula (King, 1962) is fitted on the *RDP* through *BCS* of cluster,

$$\rho(r) = \rho(0) + \frac{f_0}{1 + \left(\frac{r}{r_c}\right)^2},$$

where f_0 , r_c , $\rho(0)$ and $\rho(r)$ are peak stellar density, core-radius, background stellar density and instantaneous stellar density, respectively. The value of f_0, r_c and $\rho(0)$ for the *BCS* are found to be 5.21±0.29, 8.39±0.85 and 0.89±0.16,respectively. The resultant fit cuts the $\rho(0)$ at the outside of range of determined radial densities, therefore, we are not capable to give the value of cluster radius. The model

limiting radius of the cluster is derived from the following relation,

$$r_{limiting} = r_c \sqrt{\frac{f_0}{3\sigma} - 1}$$

where σ is the estimation error in background stellar density. Hence, the limiting radius is obtained to be 26.48±0.32 *arcmin*, which is greater than that of the observed cluster field by Janes et al. (2014). The *RDP* of *RCS* seem to be made by two plateau regions, such as, 0 < r≤7 *arcmin* and 10 < r≤17 *arcmin*. The higher stellar density of *RCS* at the core region may be appears due to the enhancement of probable super giant members of the cluster. Furthermore, the sloppy region of *RCS* is found to be at the radial distance range of 7 < r≤10 *arcmin*, which is called core-corona transition region.

5. SURFACE NUMBER DENSITY TRACER OF MASS SEGREGATION

Surface number density profile (*SNDP*) represents the stellar variation of various magnitude bin (or masses) with the radial distance and also helpful to understand the over-density inside the core-radius. The *SNDPs* of both components have been depicted in Fig. 6. The *SND* values of *BCS* indicates that massive stars are concentrated at the innermost region (0 < r≤5 arcmin) leads the evidence of mass-segregation phenomena. The *SNDPs* of *RCS* of core region shows clear separation between them and *SND* values are higher than that of the coronal region.

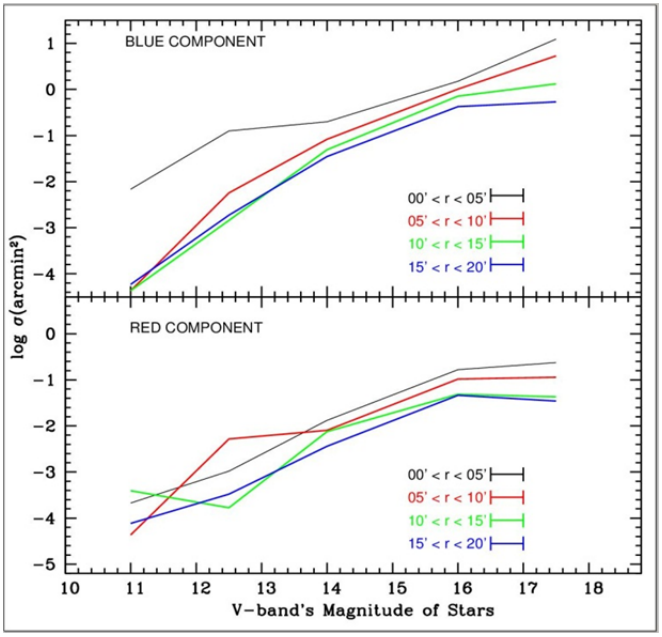

Fig. 06: The upper and lower panels are shown SNDP for BCS and RCS respectively. The surface number density is defined as the number of stars per magnitude interval in unit area (Sung et al., 1996).

The values of *SND* of massive stars are obtained to be close to each other for both category (*BCS* and *RCS*) leads an indication of similar birthing environment of massive stars with sequence evolution. The *SGM* are those massive stars, which are evaporated from the *MS* but still belong to the cluster. Perhaps, these *SGM* are increased the stellar density of *RCS* in the core of cluster and may coronal region of the cluster is free from *SGM*.

6. IDENTIFICATION OF CLUSTER GIANT STARS THROUGH STATISTICAL DISTANCE METHOD

Since, the *RCS* of core region of clusters contains the *SGM* and FS whereas the *RCS* are coronal region are only *FS* leads uniform distribution of *FS* of *RCS*. To identify the possible giant stars of the cluster, we have been applied the statistical distance algorithm [Joshi et al. (2015)] of *RCS*. The core (0 < r≤8.39 arcmin) is considered to be giant stars region and the equal areal field region, having radial distance range (10 < r≤13.05 arcmin). Here, we are used *V, B* and *I* filters instead of *J*, *H* and *K* filters and the magnitude-colour distance is taken as,

$$D_{mc} = \sqrt{\Delta_V^2 + \Delta_{BV}^2 + \Delta_{VI}^2},$$

where Δ*V*, Δ*BV* and Δ*VI* are the differences of *V* magnitude, *B-V* colourand *V-I*, respectively, between stars of field region and giant (core of cluster) region. For it, the Δ*V*, Δ*BV* and Δ*VI* have been considered to be 0.50, 0.15 and 0.15 respectively. After applying this procedure, we have found 129 giant stars among 264 *RCS* of the core region. The giant star vertical sequence presents at the colour, *(V-K)=4.0* mag of Fig. 8. In this Figure, a parallel giant star sequence of main sequence stars is also being appeared. These both giant sequences are depicted by red dots. The position of these sequence stars is indicated that the giant stars are born in a different time span and different dynamical evolution processes.

All *BCS* members are not main sequence of stars and some of them may be field stars. These stars are not possible to separate from *MS* due to following facts. Firstly, the available photometric data not cover all cluster region. Secondary, photometrc criteria (Sharma et al., 2008) do not tell about the field stars, which having colour and magnitude values in the similar order of the *MS* of cluster.

7. NO CLUE FOR DISTINGUISH OF STARS THROUGH PROPER MOTION

The cluster members are loosely gravitational bound and each member shows its individual motion, therefore, members change their location in sky with respect to each other. The exact determination of the velocity of each star is not possible through the observations but parallax used to determine the proper motion (angular displacement) of stars by using the datasets of two different time span. Here, the proper motion

values extracted from the catalogue of Roeser et al. (2010). We have been estimated the mean proper motion of *BCS* and *RCS* as (−2.02±0.15 mas/yr, −4.52±0.16 mas/yr) and (−2.18±0.25 mas/yr, -4.24±0.27 ma/syr), respectively. The mean proper motion values of both components have been computed through utilizing the proper motion value of 973 stars among 1093 *BCS* and 291 stars among 342 *RCS*, respectively. Their vector-point diagrams are shown in Fig. 7. We have not found any clear trend for separating members and field stars, such type result is also found by Bellini et al. (2010) through the study of nearby well-studied open star clusters. The mean proper motion of *RCS* has slightly differed from that of *BCS* due to field stars in *RCS*.

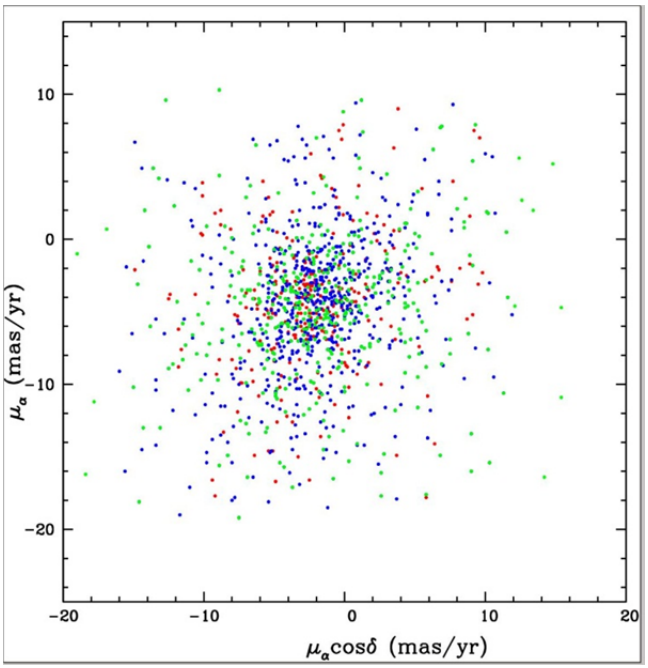

Fig. 07: The proper motion distribution of BCS and RCS is depicted by blue and red dots respectively.

The influence of field stars is large in coronal region compared to core. We have estimated the mean proper motion of the *BCS* of core using proper motion values of 411 stars which are left over after applying an iteration procedure (Joshi et al. 2014) among 458 *BCS*. The said value comes to be -1.78±0.28 mas/yr and -4.58±0.25 mas/yr in Right Ascension (*RA*) and Declination (*DEC*) directions, respectively, and these members are depicted by green dots in Fig. 7. The mean proper motion values of core and whole cluster is found to be close which suggested that the *BCS* of the cluster are less influenced by field stars.

8. DISTANCE AND AGE OF THE CLUSTER

These parameters of cluster had been already estimated by many authors (Joshi et al., 2012; Gunes et al., 2013; Janes et al., 2014). Janes et al. (2014) are computed the metallicity Z = 0.014±0.005 for this cluster through Bayesian analysis, which comes close to solar metallacity within error. By taking the new reddening value (0.12 mag) and solar metallicity, we are fitted various isochrones of various age group of Marigo's isochrone on (*V-K* vs *V*) *CMD* [Fig. 8]. Our best fitted isochrone solution provides the cluster log(age) and apparent distance modulus as 8.85±0.05 and 10.75±0.10mag respectively. The resultant distance modulus shows close agreement with the $(m\text{-}M)_V$ = 10.98±0.24 mag (Janes et al., 2014) while it is low compared to 11.15 mag (Joshi et al., 2012) and 11.33 mag (Karchenko et al., 2005). The red solid line of Fig. 8 represents the red sequence which get by the adding 0.75 mag and 0.105 mag in magnitude $(m\text{-}M)_V$ and colour *(V-K)* respectively for unresolved *MS* binaries.The heliocentric distance of the cluster is found to be 1.19±0.04 kpc through the following relation,

$$d = 10^{[(m-M)_V - R_V E(B-V)]/5+1}$$

Whenever, we have change distance modulus 10.75 mag to 11.25 mag, we have noticed that stellar numbers between sequences is increases in *(B-V)/V* and *(V-I)/V CMDs* but deceases in *(V-K)/V CMD*. Thus, data incompleteness increases between B and K bands with the distance modulus.

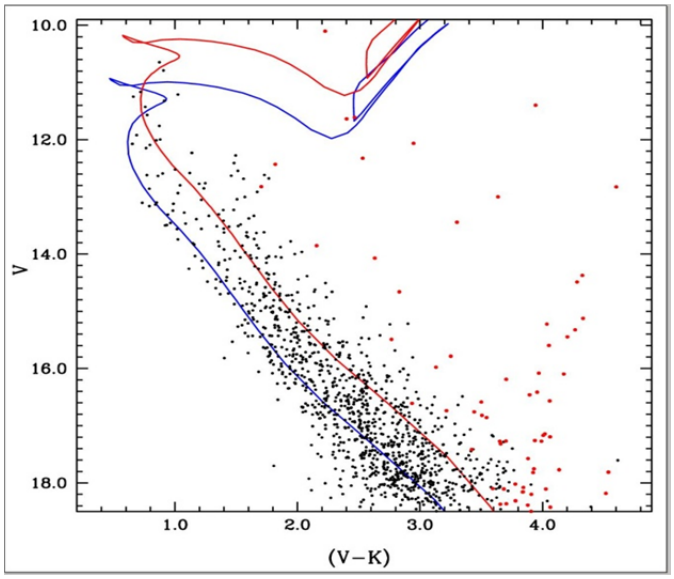

Fig. 08: ***The blue and red solid lines represent the boundary for binary stars. The blue and red lines are also showing the best fitted isochrone and red sequence of the binary stars, respectively.***

9. BCS AND MASS-FUNCTION (MF)

The *MF* is the relative number of stars per unit mass, which is computed due to the inability of measurement of initial-MF (*IMF* i.e. stellar mass distribution in per unit volume in a star formation event). The *MF* can be defined by a power law as $N\log(M) \propto M^{\Gamma}$ and its slope Γ can be determined through the following relation

$$\Gamma = \frac{d\log N(\log m)}{d\log m},$$

where N log(m) is the stellar number in per unit logarithm mass. A total of 1318 stars in (B-V)/V CMD and 538 stars in (V-K)/V CMD are found between blue and red sequences. [MF values are listed in Table 1 and shown in Fig. 9]. The least stellar number in (V-K)/V CMD indicates the data incompleteness. The Γ values of these BCS are computed to be -3.81±0.51 and -2.83±0.69 through (B-V)/V and (V-K)/V CMDs respectively. The incompleteness does not significantly alter the Γ value of cluster whereas the MF values are significantly decreased due to the incompleteness of data. The Γ value through (V-K)/V CMD is slightly increased due to large incompleteness of the data.

We are found 1111 *BCS* in *(V-K)/V CMD* which are low compare to 4088 *BCS* in (B-V)/V *CMD*. The MF values of these members have been listed in Table 2 and shown in Fig. 10. The Γ values for all *BCS* are found to be -3.80±0.11 and -3.51±0.19 through *(B-V)/V* and *(V-K)/V CMDs* respectively. To investigate the cause of low *MF* values in fainter end of both *CMD*, we have drawn *(B-V)/V CMD* and *(V-I)/V* for cluster through all archive data of Janes et al. (2014) and these *CMDs* are shown in Fig. 11.

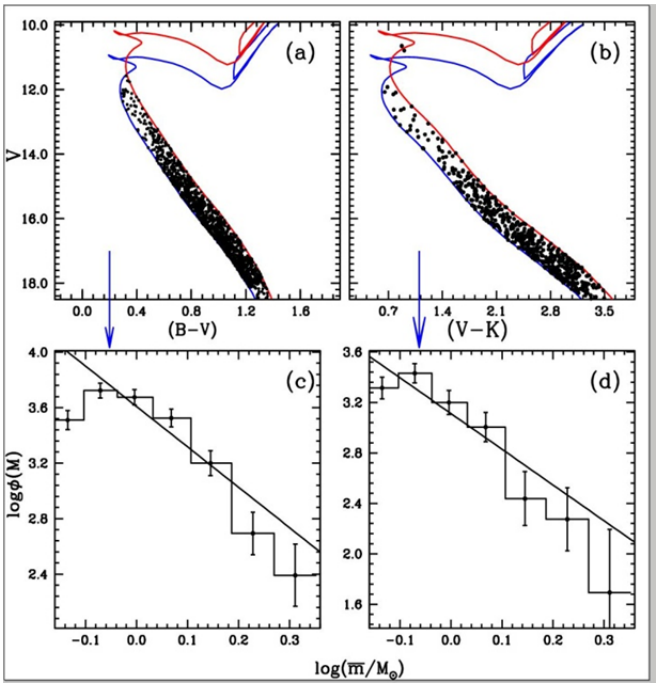

Fig. 09: The blue and red solid lines represent the boundary for binary stars in each CMD (a & b). The MF slope values estimated through these CMDs have been shown in below of them (c & d).

Table 1: The MF of the cluster NGC 6866 derived from BCS between blue a sequences in (A) $(B-V)$ vs V CMD and (B) $(V-K)$ vs V CMD (represented b A and B respectively).

V range (mag)	Mass range $M_\odot$	$\bar{m}$ $M_\odot$	$log(\bar{m})$	N_A	N_B
11.5-12.5	2.235-1.854	2.045	0.311	20	04
12.5-13.5	1.854-1.524	1.689	0.228	42	16
13.5-14.5	1.524-1.267	1.395	0.145	127	22
14.5-15.5	1.267-1.070	1.168	0.068	246	74
15.5-16.5	1.070-0.912	0.991	-0.004	328	110
16.5-17.5	0.912-0.787	0.850	-0.071	338	173
17.5-18.5	0.787-0.677	0.732	-0.135	212	135

V range	$log(\Phi)_A$	$e_{log(\Phi)_A}$	$log(\Phi)_B$	$e_{log(\Phi)_B}$
11.5-12.5	2.392	0.224	1.693	0.500
12.5-13.5	2.693	0.154	2.274	0.250
13.5-14.5	3.200	0.089	2.438	0.213
14.5-15.5	3.525	0.064	3.004	0.116
15.5-16.5	3.675	0.055	3.200	0.095
16.5-17.5	3.723	0.054	3.432	0.076
17.5-18.5	3.511	0.069	3.315	0.086

Table 2: The MF of the cluster NGC 6866 derived from BCS found in (A) $(B-$ CMD and (B) $(V-K)$ vs V CMD (represented by suffix C and D respectively).

V-mag	N_C	N_D	$log(\Phi)_C$	$log(\Phi)_D$
11.5-12.5	48	11	2.772±0.114	2.132±0.302
12.5-13.5	113	41	3.123±0.094	2.683±0.156
13.5-14.5	262	63	3.514±0.062	2.895±0.126
14.5-15.5	460	125	3.797±0.047	3.231±0.089
15.5-16.5	800	205	4.062±0.035	3.470±0.070
16.5-17.5	1265	300	4.296±0.028	3.671±0.058
17.5-18.5	1121	355	4.234±0.030	3.735±0.053

The minimum stars are appeared between 18 to 19 mag of V-band as seen in Fig. 11. As a result, the *MF* values found to be low compare to expected value. We have not found different Γ value for all *BCS* compare to that for BCS between sequences. Thus, we have considered the Γ value for cluster -3.80±0.11 which is very high from to normal Γ value (-2.35) for clusters. We are also concluded that MF study is more reliable through *BCS* compare to the binary stars sequences as comes from the photometric criteria.

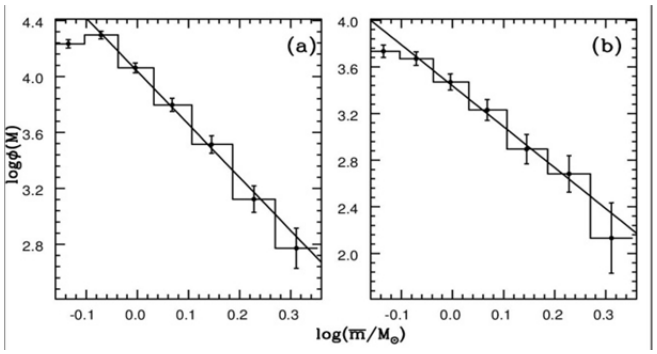

Fig. 10: The MF slope values estimated through (B-V)/V and (V-K)/V CMDs.

10. NATURE OF TOTAL-TO-SELECTIVE-EXTINCTION

We are estimated the IR interstellar extinction through the *(V-K)/(J-K) TCD* as shown in Fig. 12. In this figure, the blue solid line represents the solar metallicity isochrones of log(age)=8.85 while the red solid line is obtained by adding the 0.45 mag and 0.07 mag shift in *(V-K)* and *(J-K)* colours, respectively. Thus, the colour-excess, *E(V-K)* and *E(J-K)* for the cluster are found to be 0.45 mag and 0.07 mag, respectively, which gives the value of normal reddening vector *E(J-K)/E(V-K)* as 0.16. This vector value is low than expected value i.e. 0.173. This low value is occurred due to the presence of interstellar clouds and dust in the direction of cluster field. The reddening value of cluster is found to be 0.16 mag through the Mathis (1990) relation, *E(V-K)=2.75*. This resultant reddening value is slightly E(B-V) high compare to 0.12 mag as estimated through *(U-B)/(B-V) TCD*. These two different value of reddening suggests that the total-to-selective-extinction value for the cluster is altered from the normal value due to the either presence of dust or the data incompleteness.

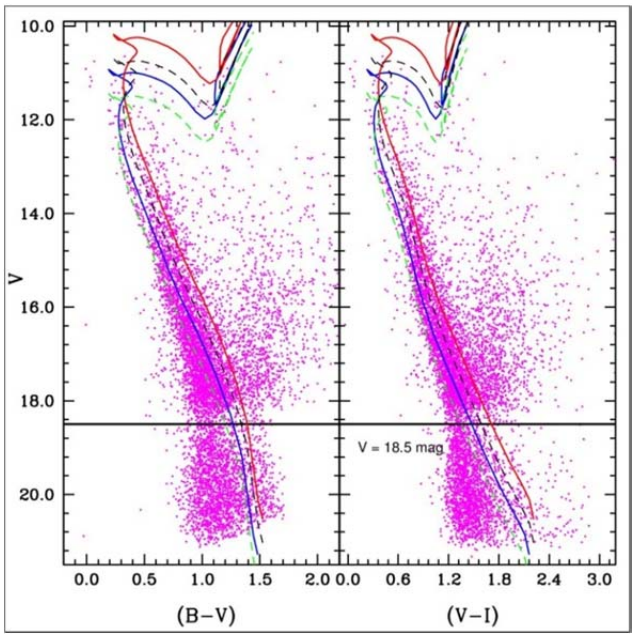

Fig. 11: The (B-V)/V CMD and (V-I)/V CMDs. The solid lines represent the boundary of blue and red sequence whenever the apparent distance modulus is 10.75 mag while dashed lines represent same for apparent distance modulus is 11.25 mag.

11. CONCLUSION

The scientific study of *OSCs* are possible due to computational statistical programs. These prescribed programs will/have written in the computational language such as *PYTHON*, *FORTRAN* etc. These programs are framed in such a way that they satisfied all scientific arguments and reduce the personal uncertainty. In the present paper, the computational algorithm has been developed for studying the parametric study of the cluster NGC6866. These computational programs are effectively used to construct/design various parametric plots through the gathered data of the cluster. The main results of present study have been prescribed as follows. On the comparison of various photometric catalogue of this cluster, the photometric procedure of Joshi et al. (2012) for estimation of the stellar magnitude seems to be less precise. Such least precision is occurred due to either the sky condition on the observational night or adopted standardization procedure. Here, the photometric catalogue of Janes et al. (2014) is used to estimate the fundamental parameters of this cluster due to its large observational field. The radial over density of cluster are occurred due to the *BCS* stars which are further supplemented by *SNDs* in various radial zones. The core-corona transition region is found as 7-10 arcmin, which would be very effective to understand the evolutionary interaction between core and corona regions of the cluster. Though the *BCS* and *RCS* are neither distinguishable in *RA-DEC* plane nor distinct proper motions, whereas they have been separated on the basis of their location on *CMD* plane. We have been also found that the *ZAMS* are not fitted on the *RCS*, whereas, *RCS* followed a linear trend. Our analysis shows that some *RCS* of core-region found to be Giant members of the cluster. The value of *MF* slope shows its dependency on the incompleteness of data. This manuscript is a mile-stone step to understand the exact members of the cluster through their known parametric values.

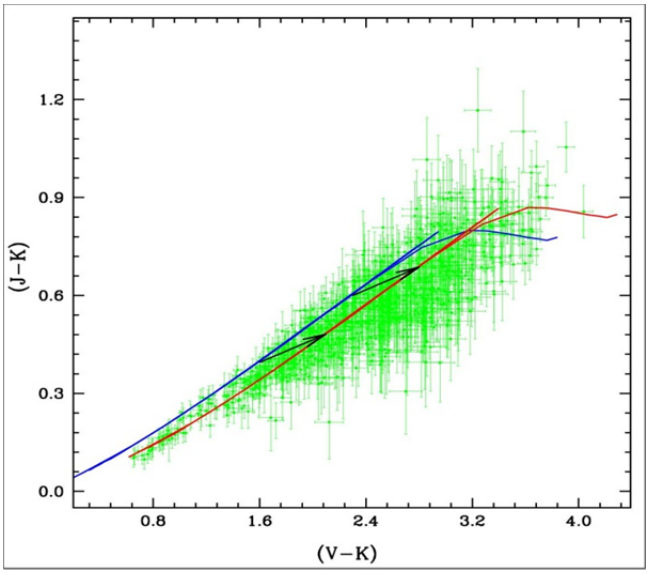

Fig. 12: The (V-K) vs (J-K) TCD for the cluster. The black solid arrows represent the normal reddening vector E(J-K)/E(V-K)=0.173. The horizontal and vertical green lines represent the errors in colours, (V-K) and (J-K).

12. ACKNOWLEDGEMENTS

This research has made use of the VizieR catalogue access tool, CDS, Strasbourg, France. The original description of the VizieR service was published in A&AS 143, 23. GCJ is also thankful to APcyber Zone (Nanakmatta) for providing computer facilities. GCJ is also thankful to Shree Nilamber Joshi for providing the friendly environment, which becomes mile stone of my research work.

REFERENCES

[1] Bellini, A., Bedin, L. R., Pichardo, B., Moreno, E., Allen, C., Piotto G., Anderson, J.: Absolute proper motion of the Galactic open cluster M 67, Astron. Astrophys., 513, 51 (2010)

[2] Bostanci, Z. F., Ak T., Yontan T., Bilir, S., Guver, T., Ak, S., et al.: A comprehensive study of the open cluster NGC 6866, Mon. Not. R. Astron. Soc., 453, 1095 (2015)

[3] Gunes, O., Karatas, Y., Bonatto, C.: Astrophysical and Structural Parameters of the Open Clusters NGC 6866, NGC 7062, and NGC 2360, Astron. J.145, 7 (2013)

[4] Kharchenko, N.V., Piskunov, A.E., Roeser, S., Schilbach, E., Schola, R.-D.: Astrophysical parameters of Galactic open clusters, Astron. Astrophys.438, 1163 (2005)

[5] Janes, K., Barnes, S.A., Meibom, S., Hoq, S.: Open Clusters in the Kepler Field, II. NGC 6866, Astron. Astro-phys.570A, 20 (2014)

[6] Joshi, Gireesh C., Joshi, Y. C., Joshi, S., Chowdhury S., Tyagi, R. K.: Complex stellar system ESO65SC03: Open cluster or remnant?, Publ. Astron. Soc. Aust. 32, 22 (2015)

[7] Joshi, Y.C., Balona, L.A., Joshi, S., Kumar, B.: Photometric Study of the open cluster-II. Stellar Population and Dynamical Evolution in NGC 559, Mon. Not. R. Astron. Soc.437, 804 (2014)

[8] Joshi, Y.C., Joshi, S., Kumar, B., Mondal, S., Balona, L.A.: Photometric study and detection of variable stars in the open clusters I. NGC 6866, Mon. Not. R. Astron. Soc. 419, 2379 (2012)

[9] King J.: The structure of star clusters.I. An empirical density law, Astron. J.67, 471 (1962)

[10] Marigo et al.: Evolution of asymptotic giant branch stars II. Optical to far-infrared isochrones with improved TP-AGB models, Astron. Astrophys.482, 883 (2008)

[11] Mathis, J. S.: Interstellar dust and extinction, Annu. Rev. Astron. Astrophys.28, 37 (1990)

[12] Roeser, S., Demleitner, M., Schilbach, E.: The PPMXL catalog of Positions and Proper Motions on the ICRS. Combining USNO-B1.0 and the Two Micron All Sky Survey (2MASS), Astron. J.139, 2440 (2010)

[13] Schmidt-Kalar Th; 1982, In: Landolt/Bornestein, Numerical Data and functional Relationship in Science and Technology, New Series, Group VI, vol 26, Scaifers K., & Voigt H. H.(eds.) Springer-Verlog, Berlin, p.14

[14] Sharma, S., Pandey, A.K., Ogura, K., Mito, H., Tarusawa, K., Sagar, R.: Wide-field CCD photometry around nine open clusters, Astron. J.132, 1669 (2006)

[15] Sharma, S., Pandey, A.K., Ogura, K., Aoki, T., Pandey, K., Sandhu, T.S., Sagar R.: Mass functions and photometric binaries in nine open clusters, Astron. J.135, 1934 (2008)

[16] Sung, H., Lee, S., Lee, M.G., Ann, H.B.: UBV CCD Photometry of Intermediate Age Open Cluster M11 I. Statistical Analysis, J. Kor. Astron. Soc.29, 269 (1996)